Supplementary Section: Nonlinear Terahertz Absorption of Graphene Plasmons

Mohammad M. Jadidi,*,† Jacob C. König-Otto,‡ Stephan Winnerl,‡ Andrei B. Sushkov,§ H. Dennis Drew,§ Thomas E. Murphy,† and Martin Mittendorff†

†*Institute for Research in Electronics & Applied Physics, University of Maryland, College Park, MD 20742, USA*

‡*Helmholtz-Zentrum Dresden-Rossendorf, PO Box 510119, D-01314 Dresden, Germany*

¶*Technische Universität Dresden, 01069 Dresden, Germany*

§*Center for Nanophysics and Advanced Materials, University of Maryland, College Park, Maryland 20742, USA*

E-mail: mmjadidi@umd.edu

Equivalent Circuit Model

When a linearly polarized plane wave is normally incident on a two-dimensional conductive sheet, the transmission, reflection, and absorption can be described using the simple transmission-line model shown in Fig. S1.

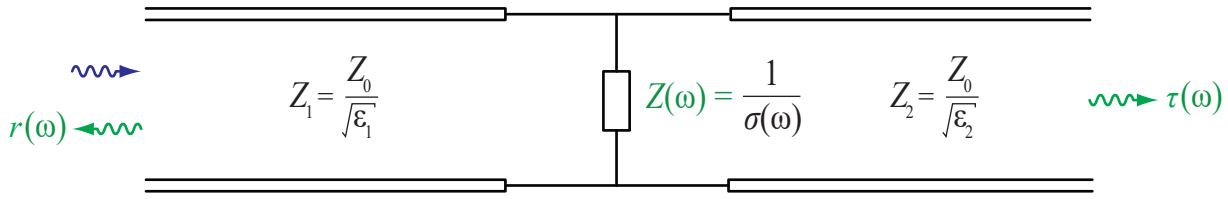

Figure S1: Transmission line model of reflection, transmission and absorption in a conductive sheet.

In this model, the incident and substrate regions are modeled as transmission lines with characteristic impedances of $Z_1 \equiv Z_0/\sqrt{\epsilon_1}$ and $Z_2 \equiv Z_0/\sqrt{\epsilon_2}$, respectively, and the two-dimensional sheet is modeled with a frequency-dependent lumped conductance $\sigma(\omega)$. For a wave incident on the sheet from region 1, the reflection, transmission and absorption are then calculated to be:

$$r(\omega) = \left|\frac{Y_1 - Y_2 - \sigma(\omega)}{Y_1 + Y_2 + \sigma(\omega)}\right|^2 \tag{S1}$$

$$\tau(\omega) = \frac{4Y_1Y_2}{\left|Y_1 + Y_2 + \sigma(\omega)\right|^2} \tag{S2}$$

$$A(\omega) = 1 - r(\omega) - \tau(\omega) = \frac{4Y_1\mathbf{Re}\{\sigma(\omega)\}}{\left|Y_1 + Y_2 + \sigma(\omega)\right|^2} \tag{S3}$$

where $Y_i = 1/Z_i$.

When experimentally measuring the linear transmission using Fourier transform infrared spectroscopy, it is conventional to normalize the transmission relative to that when the conductive sheet is absent (i.e., when $\sigma(\omega) = 0$). From (S2), we find

$$\frac{\tau(\omega)}{\tau_0} = \frac{\left|Y_1 + Y_2\right|^2}{\left|Y_1 + Y_2 + \sigma(\omega)\right|^2} = \left[1 + \frac{\sigma(\omega)}{Y_1 + Y_2}\right]^{-2} \tag{S4}$$

Drude Model

The sheet conductance of an unpatterned graphene sheet is described by a two-dimensional Drude conductivity:

$$\sigma(\omega) = \frac{D}{\pi(\Gamma - i\omega)} \tag{S5}$$

where D is the Drude weight and Γ is the momentum scattering rate. Both D and Γ are temperature dependent, but at room temperature they are related to the carrier concentration and mobility, respectively. The corresponding sheet impedance appearing in the equivalent circuit is

$$Z(\omega) = \frac{1}{\sigma(\omega)} = \frac{\pi\Gamma}{D} - i\frac{\pi\omega}{D} \equiv R - i\omega L \tag{S6}$$

where $R \equiv \pi\Gamma/D$ is the DC sheet resistance of graphene and $L \equiv \pi/D$ is the kinetic inductance, as shown in Fig. S2.

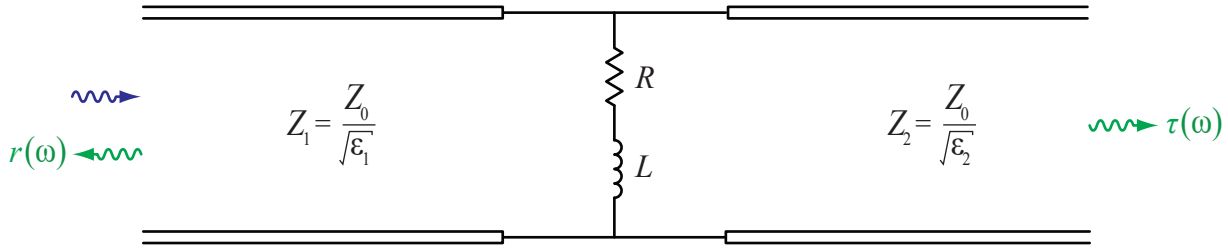

Figure S2: Equivalent circuit for Drude absorption by an unpatterned graphene sheet on a substrate.

This model correctly predicts the Drude absorption, reflection, and transmission in the terahertz regime.

Drude Lorentz Model

When a conductor is patterned into an array of ribbons with period Λ and width w, it forms a capacitive grid that can be modeled by a sheet capacitance of[1]

$$C = 2\epsilon_0\bar{\epsilon}\Lambda \ln[\sec(\pi w/2\Lambda)]/\pi \tag{S7}$$

where $\bar{\epsilon} \equiv (\epsilon_1 + \epsilon_2)/2$ is the average dielectric constant. Accounting for the sheet resistance and kinetic inductance of the graphene that comprises the ribbons, the equivalent sheet impedance may be modeled by a resistor, capacitor and inductor in series, as shown in Fig. S3:[2]

$$Z(\omega) = R\frac{\Lambda}{w} + i\omega L\frac{\Lambda}{w} - \frac{i}{\omega C} \tag{S8}$$

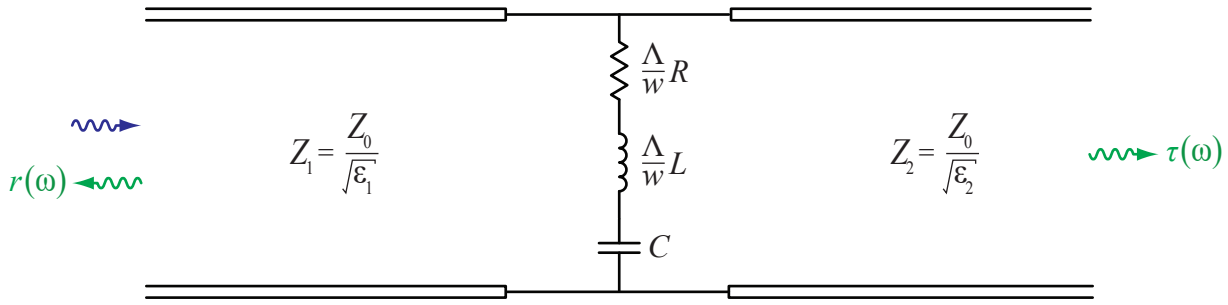

Figure S3: Equivalent circuit of graphene ribbon array.

where R and L are the graphene sheet resistance and kinetic inductance, and the additional factor of Λ/w accounts for the filling fraction of the graphene. Using the expressions for R, L and C defined in (S6) and (S7), one finds an equivalent conductivity of

$$\sigma(\omega) = \frac{1}{Z(\omega)} = \frac{w}{\Lambda}\frac{D}{\pi[\Gamma - i(\omega^2 - \omega_p^2)/\omega]} \tag{S9}$$

where the resonant (or plasmon) frequency is given by

$$\omega_p^2 \equiv \frac{Dw}{2\Lambda^2\epsilon_0\bar{\epsilon}\ln\left[\sec\left(\pi w/2\Lambda\right)\right]} \tag{S10}$$

The conductivity given in (S9) is of the same form as that obtained from the Drude-Lorentz model of conductivity for bound electrons, assuming a resonant oscillation frequency of ω_p. When incorporated into (S4), this model accurately approximates the relative transmission spectrum of the graphene ribbons.

The transmission line model presented in Figs. S1-S3 can be generalized to multilayer

and finite-thickness substrates by adding additional finite-length transmission line segments. Because the plasmon fields are highly localized near the graphene surface, we treated the oxide layer immediately below the graphene as semi-infinite for the purpose of estimating the plasmon resonance, absorption, and relative transmission. Finite element time domain simulations confirm the validity of this approximation.

Fluence Dependence

As shown in Fig. 3c, the pump-induced change in transmission $\Delta\tau$ increases approximately with the fluence $F^{1/2}$. Here we present a approximate model to explain the nature of this dependence.

The on-resonant transmission through the plasmonic ribbons can be expressed in terms of the three temperature dependent parameters D, Γ and ω_p^2 using (S2) and (S9):

$$\tau = \frac{4Y_1Y_2}{\left|Y_1 + Y_2 + \frac{w}{\Lambda}\frac{D}{\pi[\Gamma - i(\omega^2 - \omega_p^2)/\omega]}\right|^2} \tag{S11}$$

When the relative changes in these parameters are small, as is the case for the measurements reported here, the resulting fractional change in transmission $\Delta\tau/\tau$ may be approximated by Taylor-expanding (S11) to first order, with the assumption that $\omega = \omega_p$,

$$\frac{\Delta\tau}{\tau} = \frac{2\frac{w}{\Lambda}\frac{D}{\pi\Gamma}}{\left[Y_1 + Y_2 + \frac{w}{\Lambda}\frac{D}{\pi\Gamma}\right]}\left(\frac{\Delta\Gamma}{\Gamma} - \frac{\Delta D}{D}\right) \tag{S12}$$

We note that when evaluated at the resonant frequency, the thermally-induced red-shift $\Delta\omega_p^2$ causes only a higher-order change in $\Delta\tau$, which is omitted in (S12).

The Drude weight can be approximated as

$$D(T) = \frac{2e^2}{\hbar^2} k_B T \ln\left[2\cosh\left(\frac{\mu(T)}{k_B T}\right)\right] \tag{S13}$$

$$\simeq \frac{2e^2}{\hbar^2}\mu(T) \tag{S14}$$

$$\simeq \frac{2e^2\varepsilon_F}{\hbar^2}\left(1 - \frac{\pi^2 k_B^2 T^2}{6\varepsilon_F^2}\right) \tag{S15}$$

In the second line, we have used the fact that even for the hottest electron temperatures considered (660 K = 57 meV), the Fermi energy (350 meV) and chemical potential significantly exceed $k_B T$. In the third line we have employed the Sommerfeld expansion to approximate the relation between electron temperature T and chemical potential $\mu(T)$. The fractional decrease in Drude weight is then found to be:

$$\frac{\Delta D}{D} = -\frac{\pi^2 k_B^2 T^2}{6\varepsilon_F^2} \tag{S16}$$

We note that the change is estimated relative to that at absolute zero temperature, whereas in the measurements, the lattice temperature was small ($T_0 = 20$ K), but non-zero.

The scattering rate can likewise be approximated as:

$$\Gamma(T) = \frac{\Gamma_0\varepsilon_F}{\mu(T)} + \frac{\varepsilon_F V_D^2 k_B T}{4\hbar^3 v_F^2 \rho s^2} \tag{S17}$$

$$\simeq \Gamma_0\left(1 + \frac{\pi^2 k_B^2 T^2}{6\varepsilon_F^2}\right) + \frac{\varepsilon_F V_D^2 k_B T}{4\hbar^3 v_F^2 \rho s^2} \tag{S18}$$

where we have again assumed $\varepsilon_F \gg k_B T$ and employed the Sommerfeld expansion. The fraction increase in scattering rate (relative to absolute zero temperature) is then given by:

$$\frac{\Delta\Gamma}{\Gamma} = \frac{\varepsilon_F V_D^2 k_B T}{4\Gamma_0\hbar^3 v_F^2 \rho s^2} + \frac{\pi^2 k_B^2 T^2}{6\varepsilon_F^2} \tag{S19}$$

When (S16) (S19) are combined as in (S12), both effects sum to cause an increase in the

transmission that is proportional to:

$$\left(\frac{\Delta\Gamma}{\Gamma}-\frac{\Delta D}{D}\right)=\frac{\varepsilon_F V_D^2 k_B T}{4\Gamma_0\hbar^3 v_F^2\rho s^2}+\frac{\pi^2 k_B^2 T^2}{3\varepsilon_F^2} \tag{S20}$$

The first term ($\propto T$) is associated with the temperature-dependent LA phonon scattering rate, and the second term ($\propto T^2$) results from the temperature-dependent chemical potential. The relative strength of these two terms is related to the deformation potential V_D, which was adjusted to match the experimentally observed fluence dependence. For the parameters considered in the experiment, these two terms would be equal to one another at an electron temperature of $T = 336$ K. For the range of experimental conditions considered here, neither term can be neglected, and hence we expect a dependence of $\Delta\tau$ on electron temperature T that falls somewhere between linear and quadratic.

For the narrow-band terahertz pulses considered here, the relationship between peak temperature T and fluence F can be estimated by assuming that the peak temperature and peak intensity are nearly coincident in time. From equation (2) in the main text,

$$\beta T_{\max}^3 = A(\omega) I_{\max} \tag{S21}$$

where $T_{\max}$ denotes the peak electron temperature, and $I_{\max} = 0.94F/\Delta t_{\mathrm{FWHM}}$ is the peak intensity of a Gaussian pulse with fluence F and duration Δt_{FWHM}. We have again neglected the small term βT_0^3 on the left-hand side that describes the lattice temperature, and ignored the higher-order temperature-dependent change in the absorption coefficient A appearing on the right-hand side. (S21) predicts that the peak temperature will scale as $F^{1/3}$, as confirmed by the numerical simulations of Fig. 3c.

Substituting this relationship into (S20), one concludes that for the experimental conditions considered here the change in transmission $\Delta\tau$ should exhibit a non-power-law dependence on fluence that falls intermediate between $F^{1/3}$ and $F^{2/3}$. As shown in Fig. 3b, empirically observed and simulated scaling relation close to $F^{1/2}$ is consistent with this

model. We note that including the temperature-dependent LA phonon scattering in addition to conventional Coulomb impurities was essential to correctly match the observed fluence dependence.

Frequency Dependence of the Nonlinear Absorption

The increased carrier temperature changes the strength of the plasmon absorption as well as its resonance frequency. Hence, the nonlinear absorption is highly frequency dependent. While both effects lead to an increase of the transmission at resonance, the situation changes for photon frequencies below resonance. In this case, red shift of the plasmon resonance leads to a decrease of the transmission, opposed to the effect of the weakened plasmon absorption. Whether the overall change in transmission is positive or negative depends on which of these processes dominates. To investigate this behavior, we calculated the change of the transmission as a function of the probe photon frequency with the model described in the main text. The parameters of the calculation were the same as in the simulation of the experiment, only the photon frequency of the probe was varied. The calculated change in transmission as a function of the probe frequency for different pump-induced electron temperature rise is depicted in Fig. S4. Our calculations show clearly that the red shift is the dominating effect and therewith the overall pump-induced change in transmission is predicted to be negative for photon frequencies below resonance.

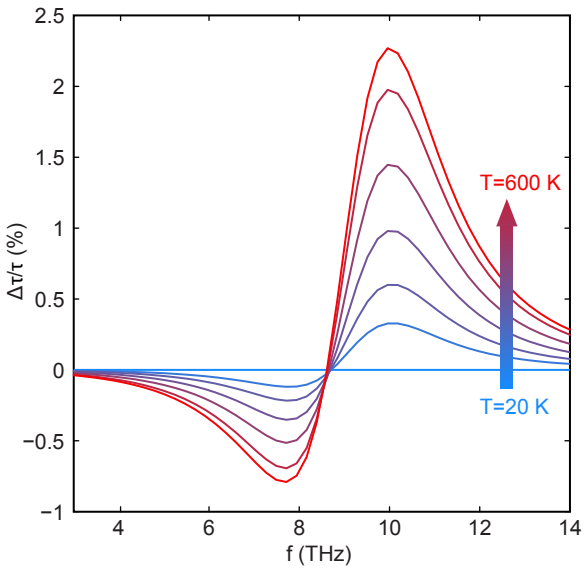

Figure S4: Peak change of transmission as function of frequency calculated for the sample used in our experiments.

References

(1) Whitbourn, L. B.; Compton., R. C. *Appl. Optics* **1985**, *24*, 217–220.

(2) Chen, P.-Y.; Alù, A. *IEEE Trans. THz Sci. Technol.* **2013**, *3*, 748–756.